Electrodeposition of Well-Adhered Multifarious Au-Particles at a Solid|Toluene|Aqueous Electrolyte Three-Phase Junction

ARTICLE *in* THE JOURNAL OF PHYSICAL CHEMISTRY C · OCTOBER 2012

Impact Factor: 4.77 · DOI: 10.1021/jp307674k

7 AUTHORS, INCLUDING:

Izabela Kaminska
Technische Universität Braunschweig
16 PUBLICATIONS **197** CITATIONS
SEE PROFILE

Martin Jönsson-Niedziolka
Polish Academy of Sciences
51 PUBLICATIONS **520** CITATIONS
SEE PROFILE

Joanna Niedziolka-Jonsson
Instytut Chemii Fizycznej PAN
68 PUBLICATIONS **1,003** CITATIONS
SEE PROFILE

THE JOURNAL OF PHYSICAL CHEMISTRY C

Article

pubs.acs.org/JPCC

Electrodeposition of Well-Adhered Multifarious Au Particles at a Solid|Toluene|Aqueous Electrolyte Three-Phase Junction

Izabela Kaminska, Martin Jonsson-Niedziolka, Agnieszka Kaminska, Marcin Pisarek, Robert Hołyst, Marcin Opallo, and Joanna Niedziolka-Jonsson*

Institute of Physical Chemistry, Polish Academy of Sciences, Kasprzaka 44/52, 01-224 Warszawa, Poland

ABSTRACT: In order to obtain uniform and reproducible surface enhanced Raman spectroscopy (SERS) platforms, a novel method for deposition of well-adhered multifarious gold particles on a tin-doped indium oxide electrode through electrogeneration at an electrode|gold compound in toluene|aqueous-electrolyte three-phase junction was developed. The electrodeposition was carried out both by double-potential-step chronoamperometry with one pulse for nucleation and one for growth of the particles, and by potentiostatic single-potential-step chronoamperometry. Both procedures give angular, multifarious Au particles with a diameter of 150 ± 40 nm. The size of the particles is independent of deposition time, after an initial growth phase, and controlled by the formation of a microemulsion at the three-phase junction. The particles are likely deposited from the microdroplets and their size is determined by the amount of gold salt in a droplet. The mechanism involves electoreduction of tetraoctylammonium tetrachloroaurate at the tin-doped indium oxide electrode followed by ion transfer across the liquid|liquid interface. The Au particles are strongly adhered to the electrode surface. The Au particle covered electrode enhances Raman scattering on the order of 10^5–10^6 times for malachite green isothiocyanate. Surface enhanced Raman spectroscopy studies reveal that the reproducibility of the Au particle deposit is excellent both between samples (<15% RSD) and across a single sample (<12% RSD). The obtained nanoparticulate deposit was also demonstrated to show electrocatalytic activity toward dioxygen reduction.

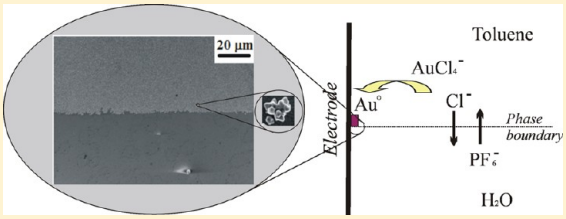

INTRODUCTION

The electrochemical processes at solid|liquid|liquid interfaces combine specific features of electron transfer at solid|liquid interfaces and ion transfer across liquid|liquid interfaces.[1] Typically a solid|liquid|liquid interface is realized by the deposition of a single or numerous redox active oil droplets on the electrode surface followed by immersion in an aqueous electrolyte.[2] The triple interface is formed at the circumference of the droplet(s). Immersion of a wire or plate electrode into a biphasic system, as shown in Figure 1, with one phase containing electrolyte and the other one containing redox active species, represents a more straightforward method which allows control of the position and the length of the three-phase junction.[3,4] The electrochemical generation of charge in the oil leads to ion transfer across the liquid|liquid interface to balance the excess charge.[3,5,6] If the oil phase initially contains only a neutral electroactive redox probe, the electrochemical reaction starts at the solid|liquid|liquid three-phase junction (purple square in Figure 1), where a large number of ions is available.[3,5,7−10] Although polar solvents, e.g., nitrobenzene, are used as the organic phase in most cases, there are examples of electrochemical redox reactions in nonpolar solvents such as kerosene[11] or toluene[12] followed by ion transfer.

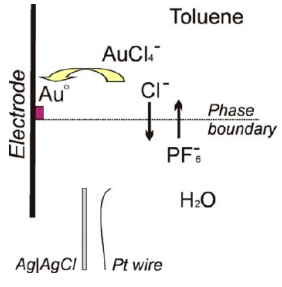

Figure 1. Scheme of the electrochemical cell and formation of the Au particle stripe.

Attempts to use the solid|liquid|liquid three-phase junction as a microreactor for electropolymerization of a monomer dissolved in the organic phase have been reported previously.[13−15] A similar arrangement was employed to deposit sol−gel processed hydrophobic silicate stripes[4] or films[16] on a flat surface. The organic phase serves as a source of the hydrophobic precursor while hydrated protons (the catalyst of the sol−gel process) are generated in the aqueous phase. A system consisting of droplets of an aqueous solution of copper salt deposited on an electrode surface immersed in a solution of 1,2-dichloroethane was applied for electrodeposition of metallic structures (copper rings).[14] Recently we have demonstrated the electrodeposition of a Au nanoparticulate stripe at a solid|ionic liquid|aqueous electrolyte interface.[17] Here we will show that metal particles can be deposited on an electrode surface also from a metal salt dissolved in a nonpolar solvent (Figure 1).

Received: August 2, 2012
Revised: September 21, 2012
Published: October 2, 2012

dx.doi.org/10.1021/jp307674k | J. Phys. Chem. C 2012, 116, 22476−22485

The application of a liquid|liquid interface for Au nanoparticle (AuNP) preparation was inspired by Faraday[18] and utilizes the chemical reduction of a metal salt dissolved in the organic phase by a hydrophilic reductant from the aqueous solution. In earlier studies the potential drives the reduction of $AuCl_4^-$ ions present in the organic phase by the hydrophilic redox active anion $Fe(CN)_6^{4-}$.[19] The electron transfer requires close proximity between the reactants which leads to the formation of AuNPs at the interface and not in the bulk solution. If the organic phase is polar, this process can be controlled by a potential applied across the liquid|liquid interface and AuNPs are deposited directly at the interface between the two immiscible electrolyte solutions (ITIES).[19−32] The transfer of $AuCl_4^-$ ions under potential control from the organic phase to an aqueous solution of monomers such as tyramine can be also employed.[22,26,27] The latter is used to reduce the gold precursor and AuNPs are embedded in a polymer film. The size of the nanoparticles can be controlled by the adjustment of the Galvani potential difference.[27] Later, the opposite design, with water-soluble metal complex ions and a hydrophobic electron transfer reagent, became more popular.[33−36] Yet another approach involves the electrochemical transfer of metal ions from the aqueous to the organic phase facilitated by hydrophobic polyphenylpyrrole monomer polymerization and the growth of metal nanoparticles is stabilized by the newly formed polymer.[37] A two-phase system was also applied for the electrodeposition of metal nanoparticles within a membrane (aluminum oxide) positioned at the liquid|liquid interface,[36] but they were not used for electrodeposition of metal on the electrode surface.

The method proposed here also involves the liquid|liquid interface and electrochemical potential control. However, the geometry of the cell and the phase composition are different from those in previous reports. The working electrode, where metal is electrodeposited, is immersed into both phases (Figure 1), but the counter and reference electrodes are immersed only into the aqueous electrolyte. This arrangement allows the use of a low polarity solvent (toluene) as a source of the gold precursor, tetraoctylammonium tetrachloroaurate ($TOAAuCl_4$), which is easy to prepare by anion exchange.[18] We show that the low polarity of the organic phase and the insolubility of the gold salt in the aqueous phase lead to the electrochemical formation of a Au deposit on the electrode close to the liquid|liquid interface. The Au deposition is accompanied by ion transfer across the liquid|liquid interface (Figure 1). We propose a mechanism where the particle deposition is influenced by the formation of a microemulsion at the three-phase junction.

The obtained gold deposit is highly stable. Contrary to AuNPs electrodeposited from a single aqueous phase, it endures ultrasonication in a bath without any changes in the number of particles at the electrode surface. This feature allows the use of electrogenerated particles at the three-phase junction in further experiments in different solvents, without any stabilizing agents. The gold deposit exhibits catalytic activity toward dioxygen reduction and, more importantly, can be applied as a sensitive platform for surface-enhanced Raman scattering (SERS).

EXPERIMENTAL SECTION

Materials and Methods. $HAuCl_4{\cdot}3H_2O$, tetraoctylammonium bromide (TOABr; 98%), and KPF_6 (98%) were obtained from Sigma-Aldrich. Toluene (analytically pure) was from Chempur. Malachite green isothiocyanate (MGITC) was from Invitrogen. Tin-doped indium oxide coated glass (ITO) (sheet resistivity 8−12 Ω/square) was obtained from Delta Technologies Ltd. All chemicals were employed without further purification. Water was filtered and demineralized with an ELIX system (Millipore).

Tetraoctylammonium tetrachloroaurate ($TOAAuCl_4$), 15 mM solution, was obtained by anion exchange from TOABr, toluene, and $HAuCl_4{\cdot}3H_2O$ aqueous solutions as described elsewhere.[18]

Scanning electron microscopy (SEM) images were obtained with a Zeiss Supra Field and FEI Nova NanoSEM 450 scanning electron microscope with FEG (field emission gun, Schottky type) systems.

Atomic force microscopy (AFM) was performed with a multimode scanning probe microscope (Bruker) using the ScanAsyst mode.

A high resolution Auger microprobe, Microlab 350 (Thermo Electron), was used to determine the chemical composition of the deposited Au particles, utilizing high resolution SEM and Auger electron spectroscopy (AES). This equipment provides lateral resolution for local chemical analysis of ∼20 nm and depth information of a few monolayers. The detailed lateral distribution of the gold signal was examined utilizing the Auger line scan function. The chemical state of surface species was identified using the high energy resolution of the Auger spherical analyzer (the energy resolution is continuously variable between 0.6 and 0.06%). AES spectra are recorded with a step of kinetic energy of 0.5 eV. The appropriate standards for AES reference spectra were also used. Avantage software (version 4.16) was used for data acquisition and processing.

SERS measurements were performed using a Renishaw InVia Raman system equipped with a He−Ne laser emitting a 632.5 nm line used as the excitation source. The light from the laser was passed through a line filter and focused on the sample mounted on an $X-Y-Z$ translation stage with a 50× microscope objective. The Raman scattered light was collected by the same objective through a holographic notch filter to block out Rayleigh scattering. An 1800 groove/mm grating was used to provide a spectral resolution of 1 cm^{-1}. The Raman scattering signal was detected by a 1024 × 256 pixel RenCam CCD detector. The SERS signal was collected from a sample of the electrodeposited Au particles left in 10^{-6} M MGITC aqueous solution for 24 h, then rinsed with pure water, and dried at room temperature. The SERS spectra were acquired using a 150 s integration time and processed with software from Renishaw (WiRE 3.2).

Electrochemical Setup. The experimental setup for gold deposition at the solid|liquid|liquid interface consists of a glass cell half-filled with 0.1 M KPF_6 ($KClO_4$ or KCl) aqueous solution and, above it, 1 mM $TOAAuCl_4$ in toluene. A thermally cleaned (at 500 °C in air) flat, 1 cm wide ITO working electrode was immersed into the aqueous phase, and then the organic phase was carefully added to ensure the formation of a well-defined three-phase junction. The ITO electrode was connected to an Autolab PGSTAT30 (Metrohm Autolab). The electrode area immersed into each phase was ca. 1 cm^2. The counter (Pt wire) and reference (Ag|AgCl) electrodes were immersed only in the aqueous phase. For the deposition experiments double-potential-step chronoamperometry and single-potential-step chronoamperometry (CA) were used. First a potential, V_1, between −1.0 and −0.5 V was

dx.doi.org/10.1021/jp307674k | J. Phys. Chem. C 2012, 116, 22476−22485

applied for 10−200 ms, and then a second pulse, V_2 = 0 V, was applied for 10−2500 s. For a single-step technique, only a potential of 0 V was applied, for the same growth times. For the dioxygen electroreduction studies the electrode prepared as described above was immersed into oxygenated or deaerated 0.5 M H_2SO_4 aqueous solution.

RESULTS AND DISCUSSION

Electrodeposition of Au Particles by Double- and Single-Potential-Step Chronoamperometry. The double-potential-step technique is an efficient method for metal particle deposition with controlled size distribution.[38−42] Typically, the first pulse is applied to form nuclei and the second is applied to control their growth. This method was earlier used for electrodeposition of Au nanoparticles from a single phase[38,41] and is here employed to the three-phase junction system. Following this methodology a more negative potential of −1.0, −0.7, and −0.5 V for nucleation was applied during 10, 20, 50, and 200 ms followed by the growth step at 0 or −0.1 V for 10, 50, 100, 500, 1500, or 2500 s. Under these conditions a strip of Au particles was deposited on the ITO surface. One can observe the formation of the deposit near the ITIES with the naked eye. Although results presented in the literature[38−42] confirm the superiority of the double-pulse-potential technique over the single-pulse one in single liquid phase systems, the deposition mechanism in a three-phase system is different. Therefore, both double- and single-pulse deposition procedures were performed.

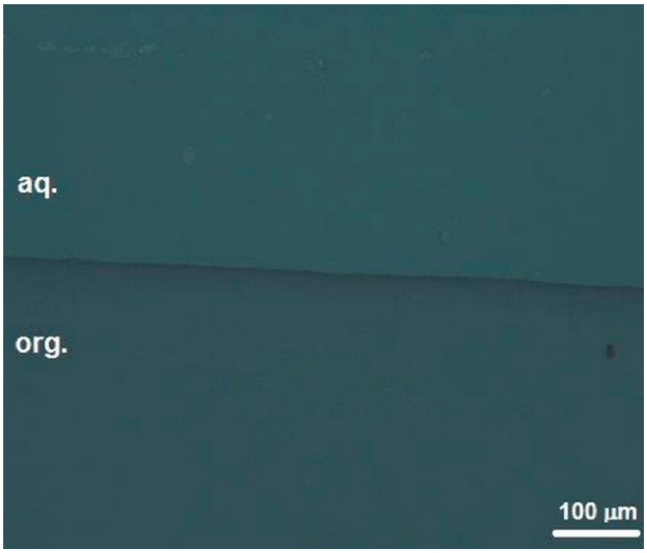

Figure 2. Optical microscope image of gold particle stripe deposited on ITO electrodes by double-potential-step chronoamperometry.

The optical microscope image (Figure 2) clearly shows that an asymmetric stripe of particulate material is formed and this asymmetry is connected to the type of the liquid phase. On the aqueous side an edge of the stripe can be clearly seen, whereas on the organic side a gradual decrease of the amount of the deposit can be found. It is also clear that the amount of material and the width of the stripe can be controlled by the electrolysis time. The asymmetry of the deposit and the time effect are likely connected to the interpenetration of the liquid phases at the three-phase ITO|liquid|liquid junction.[43]

In order to understand the mechanism of the reaction and the morphology of the deposit, additional experiments were performed. Impedance spectroscopy shows that the resistivity of the $TOAAuCl_4$ solution in toluene is very high (>100 MΩ cm), indicating negligible dissociation of the gold precursor salt in this low polarity solvent. We found it impossible to deposit any gold structures in a $TOAAuCl_4$/toluene one liquid phase system. When the cell filled with both working solutions was left for 24 h, no $AuCl_4^-$ ions were detected in the aqueous phase using UV−vis spectrometry, showing that the transfer of gold to the aqueous solution is not detectable. The behavior of this two-phase system was also studied on microscopic slides. When drops of organic and aqueous phases (covered by another glass slide) come into contact, microemulsion formation is observed and the width of the emulsion zone extends over time (Figure 3).[43−45] We measured the contact angle before, during, and after the electrochemical experiments. Its value is 27 ± 5°, and no visible change of the angle nor of the shape of the meniscus is observed for the duration of the experiment.

Clearly the formation of the gold stripe results from the geometry of the electrochemical cell, the ionic conductivity of aqueous phase, and the solubility of the gold precursor in the organic phase. Therefore, $TOAAuCl_4$ ions—exclusively present in pure toluene—are electroreduced at the three-phase junction:

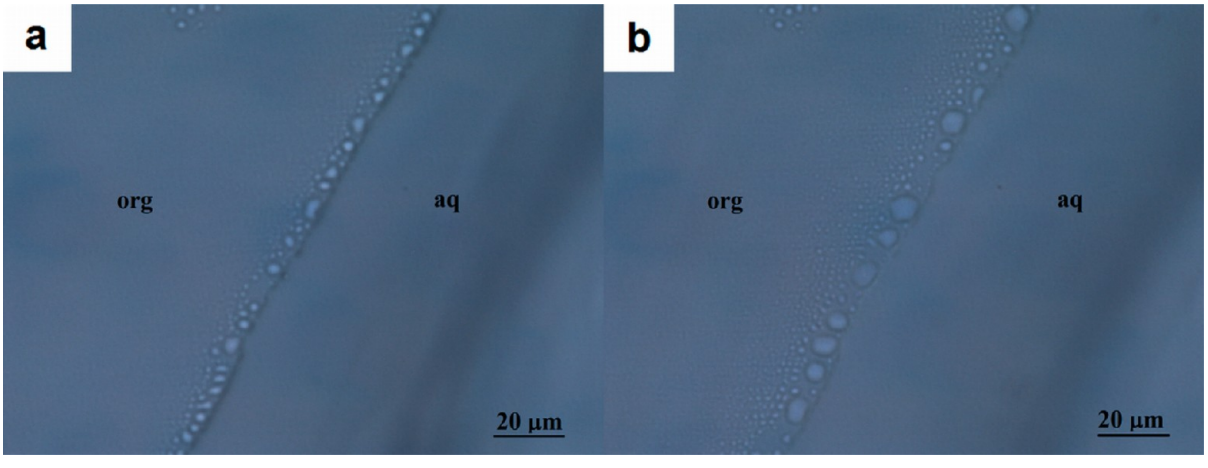

Figure 3. Microemulsion formation at the toluene|water junction shortly after toluene and water drops came into contact (a) and after ca. 50 s (b).

dx.doi.org/10.1021/jp307674k | J. Phys. Chem. C 2012, 116, 22476−22485

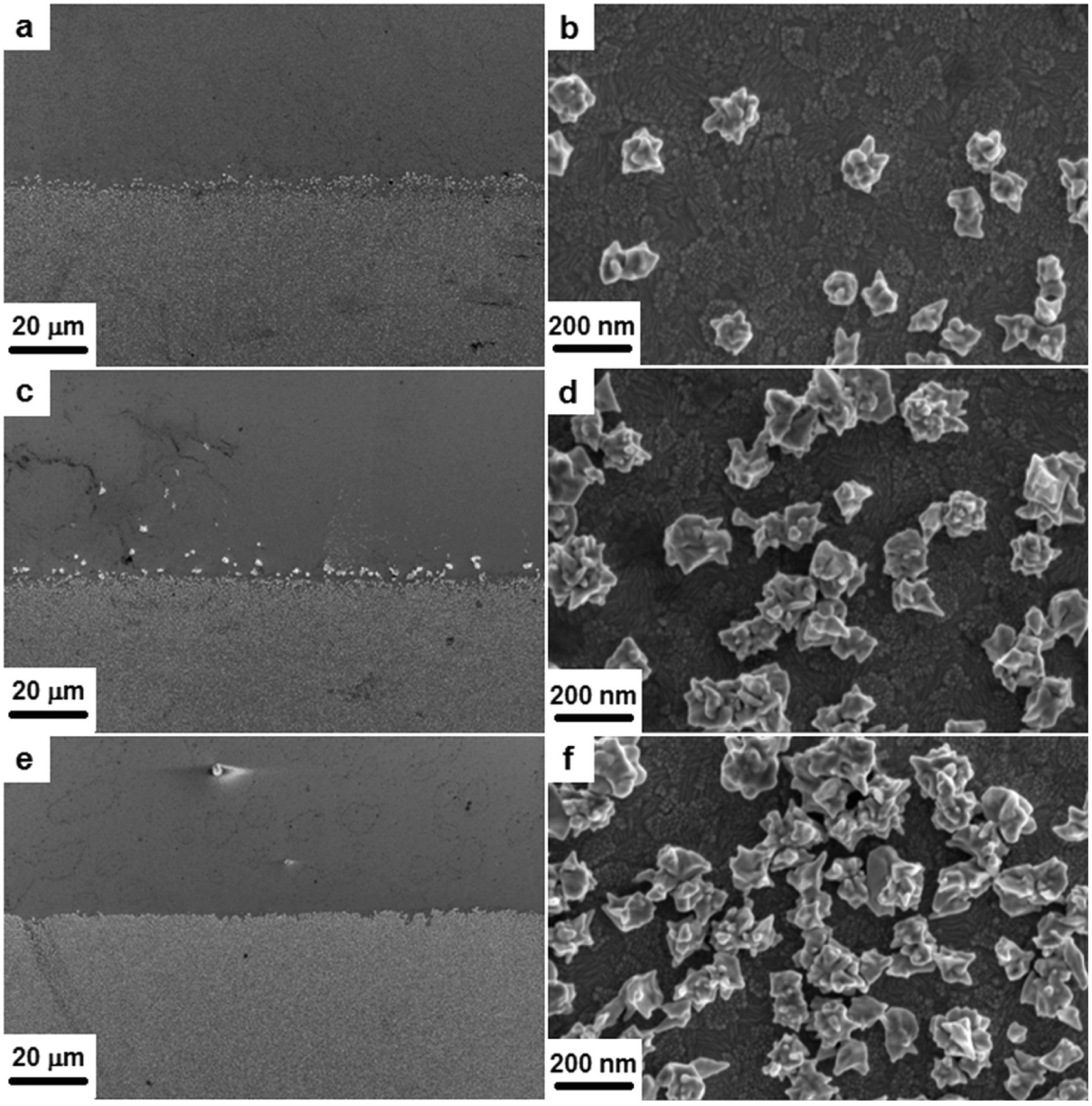

Figure 4. SEM images of gold deposit on ITO electrode obtained by double-potential-step chronoamperometry with the first potential step at −0.7 V for 50 ms and the second one shifted to 0 V for (a, b) 500, (c, d) 1500, and (e, f) 2500 s.

$$TOAAuCl_{4(org)} + 3e^-_{(electrode)} \rightarrow Au^0_{(s)} + 4Cl^-_{(org)} + TOA^+_{(org)} \quad (1)$$

Both formed ions can be expelled into the aqueous phase:

$$4Cl^-_{(org)} + TOA^+_{(org)} \rightarrow 4Cl^-_{(aq)} + TOA^+_{(aq)} \quad (2)$$

However, it is more probable that the TOA^+ stays in the organic phase and the hydrophilic chloride anions are replaced by the more hydrophobic hexafluorophosphate from the aqueous phase (Figure 1):[3,6]

$$Cl^-_{(org)} + PF_6^-{}_{(aq)} \rightarrow Cl^-_{(aq)} + PF_6^-{}_{(org)} \quad (3)$$

To test this hypothesis, hydrophobic hexafluorophosphate (standard transfer potential from water into the organic phase, $\Delta^{org}_{aq}\varphi^0_{PF_6^-} = 0$ V) was replaced by more hydrophilic anions, perchlorate ($\Delta^{org}_{aq}\varphi^0_{ClO_4^-} = 0.083$ V) or chloride ($\Delta^{org}_{aq}\varphi^0_{Cl^-} = 0.324$ V).[6,9,10,12] In the presence of ClO_4^- the stripe was significantly less dense and narrower compared to PF_6^-. In the case of Cl^- the stripe was not formed at all. This indicates that anion exchange reaction 3 indeed occurs.

SEM images (Figure 4) confirmed the formation of the asymmetric deposits consisting of Au particles with multifarious surfaces. Probably the sharp edge corresponds to the original position of the three-phase junction, because of the low polarity of the toluene phase and the lack of gold precursor in the aqueous phase (see above). The time of growth has a significant influence on the surface density and width of the particulate deposit. Its density is greater for longer electrolysis time and reaches 30−35 particles μm^{-2}. The width of the particulate stripe of relatively uniform density ranges from a few hundred (for t_1 = 10 s) to several hundred micrometers (for t_2 = 2500 s). This effect likely results from the reported emulsion formation at the liquid|liquid interface of three-phase junctions[43−45] (Figure 3). The broadening of the Au particle

dx.doi.org/10.1021/jp307674k | J. Phys. Chem. C 2012, 116, 22476−22485

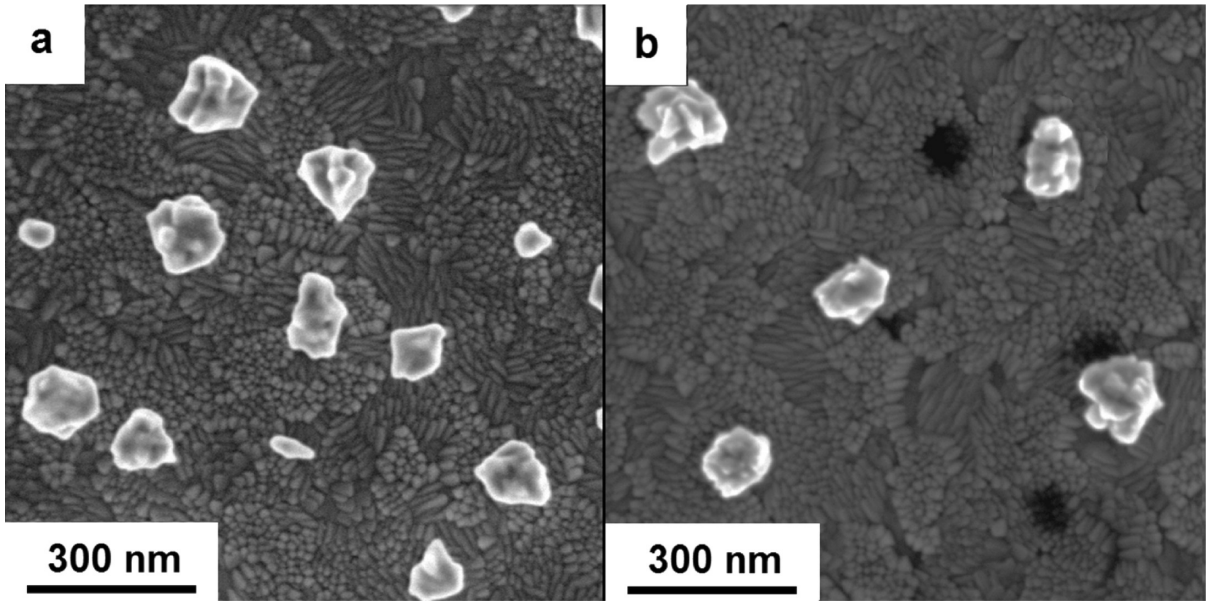

Figure 5. SEM images of gold deposit on ITO electrode obtained by (a) double-potential-step chronoamperometry (V_1 = −0.7 V for 50 ms and V_2 = 0 V for 100 s) and (b) single-potential-step chronoamperometry (at 0 V for 100 s).

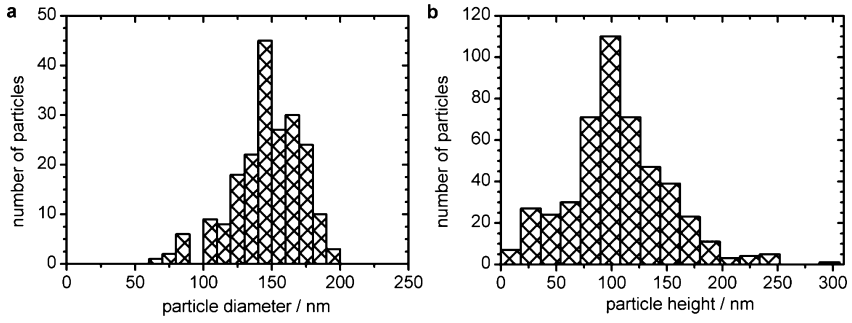

Figure 6. Size (a) and height (b) distribution of gold particles obtained by double-potential-step chronoamperometry at the three-phase junction. The potential program consists of two steps: −0.7 V for 50 ms followed by 0 V for 2500 s.

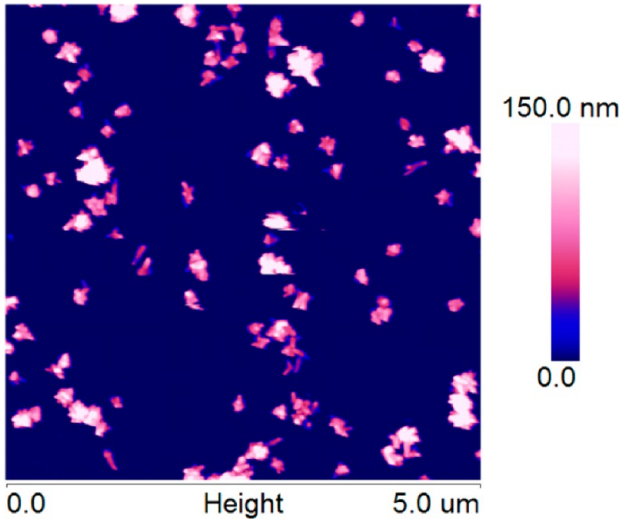

Figure 7. AFM image of gold deposit on ITO electrode obtained by double-potential-step chronoamperometry: V_1 = −0.7 V for 50 ms and V_2 = 0 V for 1500 s.

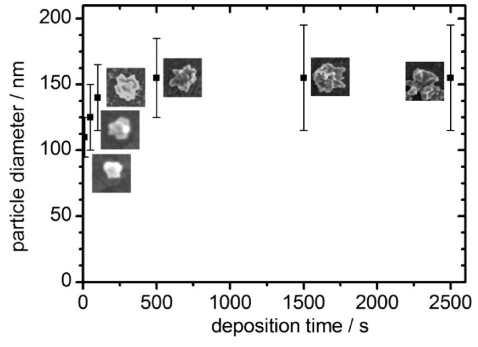

Figure 8. Diameter of gold particles as a function of growth time, for times between 10 and 2500 s. The inserted SEM images show gold particles obtained at given deposition times. The magnification of each image is the same, and each square has a side of 200 nm.

stripe can be explained by growth of the emulsion zone either spontaneously or under potential control.[43] Such solvent interpenetration prevents the formation of very narrow deposits. Indeed, tens of micrometers was earlier reported as a lowest limit for the formation of conducting polymer[13] or silicate[4] stripes at electrodelliquidlliquid three-phase junctions.

Surprisingly, nanoparticulate stripes obtained by a single-pulse potentiostatic technique were very similar to those obtained with double-pulse chronoamperometry. Both optical (not shown) and SEM images (Figure 5) showed that not only

dx.doi.org/10.1021/jp307674k | J. Phys. Chem. C 2012, 116, 22476−22485

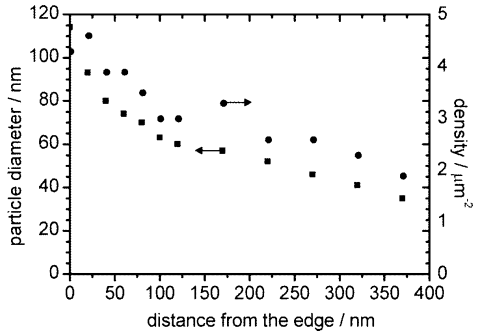

Figure 9. Size (■) and density (●) as a function of distance measured from the edge of the stripe obtained by double-potential-step chronoamperometry: V_1 = −0.7 V for 50 ms and V_2 = 0 V for 10 s.

the sizes and densities of the deposits but also the shapes of the gold particles are similar. The difference between previously published results and our results is a consequence of the influence of the three-phase junction. The deposition process is strongly influenced by the conditions at the boundary; for example, the size and density of the gold deposit are dependent on the anion used in electrolyte. What is more, the reaction is strictly limited to the area close to the three-phase junction. To be sure that the nucleation step is not crucial, we also prepared an experiment in which nucleation and growth steps were reversed, which means that the first pulse was applied at a more positive potential than the second pulse. Also, for this protocol, the features of our deposit were similar to the two methods presented above.

The size distribution of the Au particles is rather narrow (Figure 6). Their diameter is 150 ± 40 nm, and the height is 105 ± 40 nm (Figures 4–7). The diameter and height were measured from SEM and AFM images, respectively, using an automated procedure written for the free software ImageJ. The structure of the Au particles is highly angular with sharp edges (Figure 4b,d,f).

The effect of the deposition time on size and the shape of the particles, as well as the density of the deposit, was investigated. The obtained results show that not only the particle density but also their diameter decreases with shorter deposition time. From SEM images we measured the particle size, and for the shortest time that was used, the average diameter went down to 110 ± 15 nm. We also noticed that the deposition time influences the shape of the particles; for less than 100 s they are not only smaller but also more rounded. The electrogenerated gold structures develop into multifarious shapes over time until between 100 and 500 s, after which the size and shape stay constant (Figure 8).

Investigation of the size and the density of the deposited particles as a function of the distance from the three-phase junctions shows that both parameters are smaller further from the edge of the deposit. In correspondence with the measurements at short deposition times the smaller particles, found far from the edge, are more rounded than the ones closer to the edge (Figures 8 and 9). This is consistent with a model where the growth is controlled by the formation of a microemulsion at the three-phase junction. If the particles are formed from small droplets, that can explain why the size of the deposited particles is independent of the deposition time after an initial growth phase since the particle size is determined by the amount of gold salt contained in a droplet. Over time the aqueous phase extends further into the organic phase, moving the growth zone. This movement might be similar to the well-known phenomenon of a creeping electrolyte film into the capillary of dropping mercury electrodes.[46] Estimated from the size of the particles, they are each formed from about 150 fL of gold salt containing organic solvent. This corresponds quite well to the size of the domains formed seen in Figure 3, before the droplets aggregate into large drops.

The adherence of the Au particles to the electrode surface is important from the point of view of future applications. The particles in our stripes withstand at least 15 min ultrasonication in water without any decrease in the amount of deposited material, which was confirmed by SEM imaging (Figure 10). This is not the case of Au particles deposited from only a single aqueous solution by the standard double-potential-step technique, which are easily removed from the surface. The Au particles obtained at the three-phase junction also do not aggregate during the rinsing and drying processes even though they are not covered by, e.g., an organic stabilizing layer.

Two high resolution Auger spectra (Figure 11), taken from the points marked on the SEM image, are compared with a high resolution elemental Au (MNN) reference spectrum. This shows that metallic Au particles are deposited at the surface. To obtain a qualitative distribution of Au signal within a typical

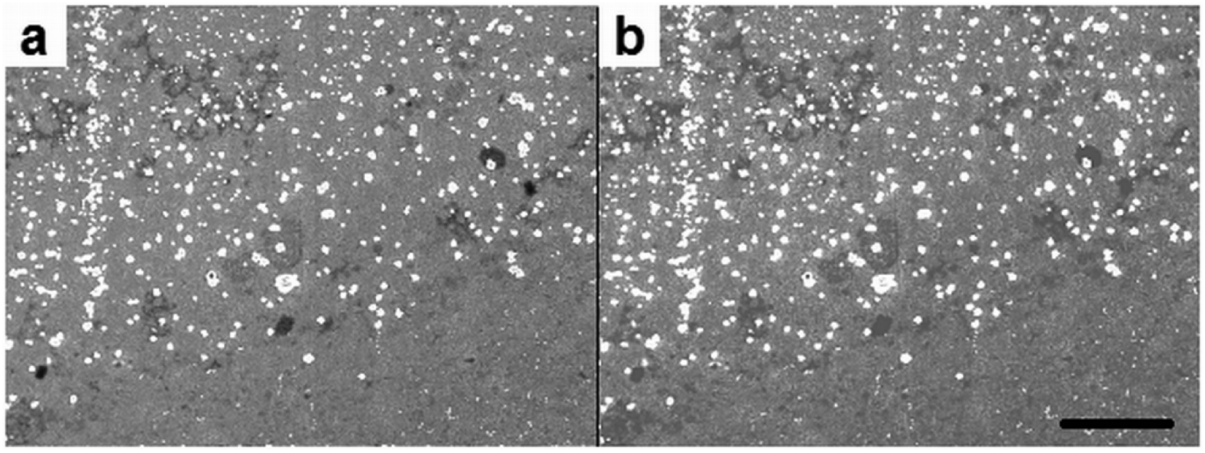

Figure 10. SEM images of gold deposit on ITO electrode obtained by double-potential-step chronoamperometry at a three-phase junction (V_1 = −0.7 V for 50 ms, V_2 = 0 V for 500 s) obtained (a) before and (b) after ultrasonication treatment. The scale bar is 2.5 µm.

dx.doi.org/10.1021/jp307674k | J. Phys. Chem. C 2012, 116, 22476–22485

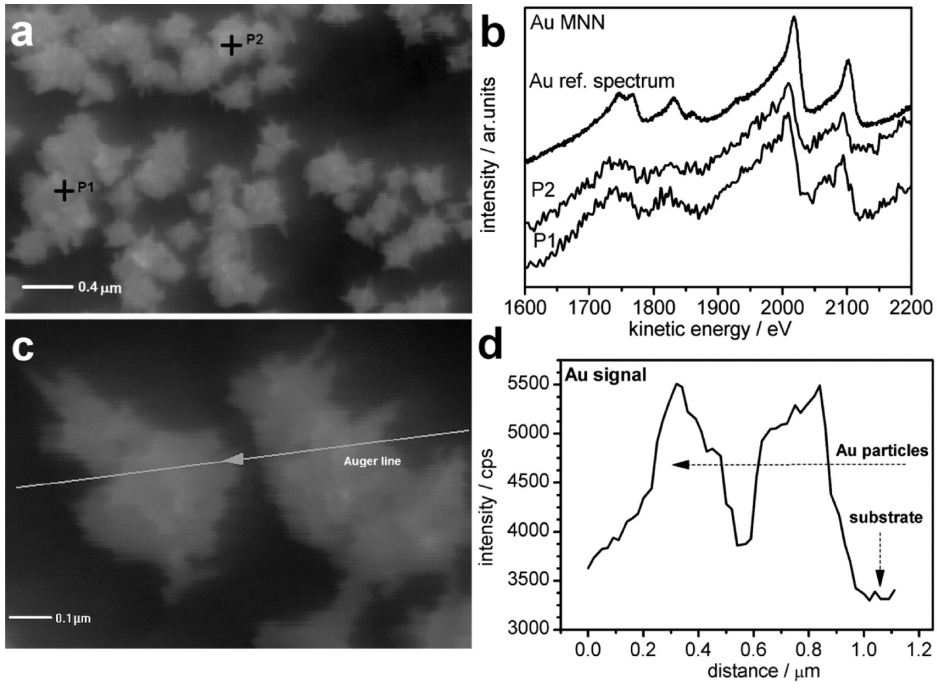

Figure 11. (a and c) SEM images of Au particles deposited on the ITO substrate. (b) High energy resolution Auger Au MNN spectra recorded at points P1 and P2 and at Au reference. (d) Auger line analysis recorded across two gold particles.

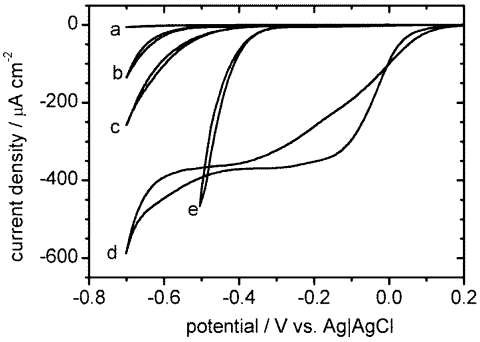

Figure 12. Cyclic voltammograms obtained in deareated and dioxygen saturated 0.5 M $H_2SO_{4\ aq}$ at a bare ITO electrode (a and b) or an electrode with electrodeposited Au particles (c and d). Geometric surface area 0.2 cm^2; scan rate 0.01 V s^{-1}. Curve e shows the response in dioxygen from a flat gold disk electrode.

particle, a line scan AES analysis was performed across several deposits (Figure 11c,d). The line scan revealed that the signal intensity of Au (MNN) drastically increases in the place of deposited particles.

Electrocatalytic Activity of Au Particles. The electrochemical properties of the Au particulate stripes were tested in oxygen saturated acidic solution. The shape of the voltammetric curve is similar to that obtained with other electrodes modified with Au particles under similar conditions (Figure 12).[47,48] The onset potential is shifted from ca. −0.4 V to ca. 0.1 V in comparison to a bare ITO electrode. The good oxygen reduction catalysis shows that the particles have good electric contact with the electrode surface.

Application of the Obtained Surface for SERS. To investigate the SERS properties of the Au particles, malachite green isothiocyanate (MGITC) was tested as a model compound. Figure 13a−f shows typical SERS spectra of MGITC adsorbed on the Au particle deposit recorded for different spots of the sample.

The position and intensity of all modes corresponding to MGITC (417, 426, 722, 907, 1167, 1365, 1582, and 1610 cm^{-1})[49] show remarkably little intrasample variability (Figure

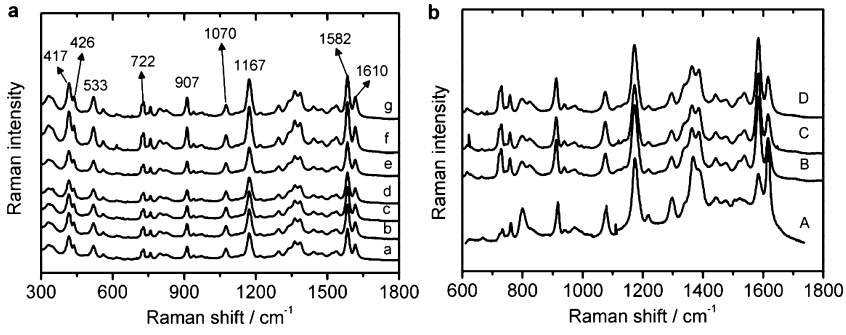

Figure 13. (a−f) SERS spectra of malachite green isothiocyanate recorded at different spots on the Au particle deposit (a, left)and different, independently prepared (A, B, C, D) Au particulate deposits (b, right). Spectra were normalized relative to the Si intensity and offset on the intensity scale for clarity.

dx.doi.org/10.1021/jp307674k | J. Phys. Chem. C 2012, 116, 22476−22485

13a, left). The standard deviation of the relative intensity of the 1167 cm^{-1} MGITC mode is less than 12% for 100 randomly distributed locations across a single sample surface.

For application purposes a SERS substrate should have good stability and reproducibility both across a single substrate and between different substrates. Figure 13b (right) illustrates Raman spectra recorded from different, separately prepared, Au particle deposits. The spectra were acquired by accumulating two spectra at 15 s integration each from randomly selected regions of the surface. The SERS signals taken at four samples are quite consistent in intensity and shape. For example, the intensity of mode observed at 1582 cm^{-1} varies by less than 15% between the A, B, C, and D surfaces.

To estimate the enhancement ability of the obtained structure, the surface enhancement factor (EF) was calculated according to the formula

$$\mathrm{EF} = \frac{I_{\mathrm{SERS}} N_{\mathrm{NR}}}{I_{\mathrm{NR}} N_{\mathrm{SERS}}} \quad (4)$$

where N_{NR} and N_{SERS} are the number of molecules probed by regular Raman spectroscopy and SERS, respectively, and I_{NR} and I_{SERS} are the corresponding intensities. I_{NR} and I_{SERS} were measured at 1167 cm^{-1} (ν_9 benzene in-plane mode).

The SERS samples were prepared by dipping the substrate in 9.0 mL of 1.0×10^{-6} M solution of MGITC. From the data of the relative intensity and the number of molecules sampled from the regular Raman and SERS measurements, the calculated EF value is from 10^5 to 10^6.

CONCLUSIONS

We have shown that a mechanically stable wide stripe of Au nanoparticles can be obtained by electrodeposition at a three-phase junction and proposed a mechanism for the deposition process. We also show that the Au particles can be used as a efficient platform for SERS. The multifarious particles are deposited at the electrode|toluene|aqueous electrolyte three-phase junction. This method employs a solution of gold salt in a hydrophobic solvent of low polarity as a reservoir for the substrate, whereas the aqueous phase serves as a source of counterions. Clearly an ionically conductive organic phase is not necessary[17] and perhaps any hydrophobic solvent capable of dissolving gold salt can be applied. Still electrochemical control is exerted by the electrochemical reduction of gold precursor from the nonconductive reservoir. This approach is also different from earlier reported electrodeposition at ITIES where, to achieve electrochemical control, a potential was applied across the liquid|liquid interface and a polar solvent has to be used as the organic phase.[19−23,25−32] Although a liquid|liquid interface is involved, the particles are deposited at the solid conductive substrate. This cell arrangement results in a specific geometry of the deposit, and the width of the stripe and the surface density of the deposit can be controlled by the time of electrolysis. The size of the particles is independent of the growth time after an initial growth phase. Likely the particle size is given by the amount of gold salt in the microemulsion droplets. The Au particles obtained by the described method show very little agglomeration and are well adhered to the surface, even resistant to ultrasonication treatment, which is a significant improvement when compared with electrodeposition from an aqueous phase and a major advantage in the use as a SERS platform. The electrodeposited, angular AuNPs with sharp points exhibit electrocatalytic properties to dioxygen reduction and show surface enhancement of Raman scattering (EF up to 10^6) with excellent reproducibility of the Au particle deposit both between samples (<15% relative standard deviation (RSD)) and across a single sample (<12% RSD). This opens the way for efficient and economical preparation of sensitive SERS platforms.

APPENDIX

The number of molecules contained in the solution was 5.4×10^{15} [$(6.02 \times 10^{23}$ molecules/mol$)(9.0 \times 10^{-3}$ L$)(1.0 \times 10^{-6}$ mol/L$) = 5.4 \times 10^{15}$ molecules]. The surface area irradiated by a laser beam (5 μm in diameter) was 19.6−20 μm^2 [$(3.14)(2.5^2$ μm$) = 19.6$ μm^2]. Therefore, around 4.2×10^6 molecules were present in the laser beam spot [$(5.4 \times 10^{15})(19.6$ $\mu m^2)/(0.25$ $cm^2)$]. The normal Raman spectrum was observed for a cell filled with pure MGITC (M = 485.98 g/mol) of density 1.014 g/cm^3. The effective illuminated volume for our setup is 22 μm^3. This value was confirmed by registering the Raman spectra of silicon while varying the distance from the focal plane. Under these conditions, $N_{NR} = 2.7 \times 10^{12}$ molecules were irradiated by the laser [$(22$ $\mu m^3)(1.014$ g/$cm^3)(6.02 \times 10^{23}$ molecules/mol$)/(485.98$ g/mol)].

AUTHOR INFORMATION

Corresponding Author

*E-mail: jniedziolka@ichf.edu.pl.

Author Contributions

The manuscript was written through contributions of all authors. All authors have given approval to the final version of the manuscript.

Notes

The authors declare no competing financial interest.

ACKNOWLEDGMENTS

The authors thank Dr. Janusz Stafiej for fruitful discussions. The work of I.K. was realized within the International Ph.D. Projects Programme of the Foundation for Polish Science. J.N.-J. thanks the Foundation for Polish Science for financial support through the FOCUS Programme No. 3/2010. Access to SEM was funded by the EC 7.FP under the Research Potential (Coordination and Support Actions FP7-REGPOT-CT-2011-285949-NOBLESSE) and to AFM by the Foundation for Polish Science under FOCUS Grant FG 3/2010.

REFERENCES

(1) Marken, F. Electrifying interfaces. *Philos. Trans. R. Soc. London, A* **2004**, *362* (1825), 2611−2633.

(2) Scholz, F.; Schroder, U.; Gulaboski, R. *Electrochemistry of Immobilized Particles and Droplets*; Springer: Berlin, 2005.

(3) Bak, E.; Donten, M.; Stojek, Z. Three-phase electrochemistry with a cylindrical microelectrode. *Electrochem. Commun.* **2005**, *7* (5), 483−489.

(4) Niedziolka, J.; Opallo, M. Electrochemically assisted sol-gel process at a three phase junction. *Electrochem. Commun.* **2008**, *10*, 1445−1447.

(5) Marken, F.; Webster, R. D.; Bull, S. D.; Davies, S. G. Redox processes in microdroplets studied by voltammetry, microscopy, and ESR spectroscopy: oxidation of N,N,N′,N′-tetrahexylphenylene diamine deposited on solid electrode surfaces and immersed in aqueous electrolyte solution. *J. Electroanal. Chem.* **1997**, *437* (1−2), 209−218.

(6) Scholz, F.; Gulaboski, R. Determining the Gibbs energy of ion transfer across water-organic liquid interfaces with three-phase electrodes. *ChemPhysChem* **2005**, *6* (1), 16−28.

(7) Aoki, K.; Tasakorn, P.; Chen, J. Y. Electrode reactions at submicron oil vertical bar water vertical bar electrode interfaces. *J. Electroanal. Chem.* **2003**, *542*, 51−60.
(8) Rayner, D.; Fietkau, N.; Streeter, I.; Marken, F.; Buckley, B. R.; Page, P. C. B.; del Campo, J.; Mas, R.; Munoz, F. X.; Compton, R. G. Electrochemical investigation of hemispherical microdroplets of N,N-didodecyl-N′,N′-diethylphenylenediamine immobilized as regular arrays on partially-blocked electrodes: A new approach to liquid vertical bar liquid voltammetry. *J. Phys. Chem. C* **2007**, *111* (27), 9992−10002.
(9) Wadhawan, J. D.; Evans, R. G.; Banks, C. E.; Wilkins, S. J.; France, R. R.; Oldham, N. J.; Fairbanks, A. J.; Wood, B.; Walton, D. J.; Schroder, U.; Compton, R. G. Voltammetry of electroactive oil droplets: Electrochemically-induced ion insertion, expulsion and reaction processes at microdroplets of N,N,N′,N′-tetraalkyl-para-phenylenediamines (TRPD, R = n-butyl, n-hexyl, n-heptyl-and n-nonyl). *J. Phys. Chem. B* **2002**, *106* (37), 9619−9632.
(10) Schroder, U.; Wadhawan, J.; Evans, R. G.; Compton, R. G.; Wood, B.; Walton, D. J.; France, R. R.; Marken, F.; Bulman Page, P. C.; Hayman, C. M. Probing Thermodynamic Aspects of Electrochemically Driven Ion-Transfer Processes Across Liquid|Liquid Interfaces: Pure versus Diluted Redox Liquids. *J. Phys. Chem. B* **2002**, *106* (34), 8697−8704.
(11) Munoz, R. A. A.; Banks, C. E.; Davies, T. J.; Angnes, L.; Compton, R. G. Electrochemistry Inside Microdroplets of Kerosene: Electroanalysis of (Methylcyclopentadienyl) Manganese(I) Tricarbonyl(I). *Electroanalysis* **2006**, *18* (6), 621−626.
(12) Shul, G.; Adamiak, W.; Opallo, M. Ion insertion into ionic liquid supported toluene generated by electrochemical redox reaction. *Electrochem. Commun.* **2008**, *10* (8), 1201−1204.
(13) Bak, E.; Donten, M. L.; Donten, M.; Stojek, Z. Electrodeposition of polymer next to the three-phase boundary. *Electrochem. Commun.* **2005**, *7* (11), 1098−1104.
(14) Davies, T. J.; Wilkins, S. J.; Compton, R. G. The electrochemistry of redox systems within immobilised water droplets. *J. Electroanal. Chem.* **2006**, *586* (2), 260−275.
(15) Gergely, A.; Inzelt, G. Electropolymerization of 3-methylthiophene at liquid 3-methylthiophene|aqueous solution|graphite three-phase junction. *Electrochem. Commun.* **2001**, *3* (12), 753−757.
(16) Niedziolka-Jonsson, J.; Jonsson-Niedziolka, M.; Nogala, W.; Palys, B. Electrosynthesis of thin sol-gel films at a three-phase junction. *Electrochim. Acta* **2011**, *56*, 3311−3316.
(17) Kaminska, I.; Niedziolka-Jonsson, J.; Roguska, A.; Opallo, M. Electrodeposition of gold nanoparticles at a solidionic liquidaqueous electrolyte three-phase junction. *Electrochem. Commun.* **2010**, *12* (12), 1742−1745.
(18) Brust, M.; Walker, M.; Bethell, D.; Schiffrin, D. J.; Whyman, R. J. Synthesis of Thiol-Derivatized Gold Nanoparticles in Two Phase Liquid-Liquid System. *J. Chem. Soc., Chem. Commun.* **1994**, 801−802.
(19) Cheng, Y. F.; Schiffrin, D. J. Electrodeposition of metallic gold clusters at the water/1,2-dichloroethane interface. *J. Chem. Soc., Faraday Trans.* **1996**, *92* (20), 3865−3871.
(20) Binder, W. H. Supramolecular assembly of nanoparticles at liquid-liquid interfaces. *Angew. Chem., Int. Ed.* **2005**, *44* (33), 5172−5175.
(21) Campbell, A. I.; Dryfe, R. A. W.; Haw, M. D. Deposition and Aggregation of Au at the Liquid/Liquid Interface. *Anal. Sci.* **2009**, *25* (2), 307−310.
(22) Knake, R.; Fahmi, A. W.; Tofail, S. A. M.; Clohessy, J.; Mihov, M.; Cunnane, V. J. Electrochemical nucleation of gold nanoparticles in a polymer film at a liquid-liquid interface. *Langmuir* **2005**, *21* (3), 1001−1008.
(23) Kumar, A.; Mandal, S.; Mathew, S. P.; Selvakannan, P. R.; Mandale, A. B.; Chaudhari, R. V.; Sastry, M. Benzene- and anthracene-mediated assembly of gold nanoparticles at the liquid-liquid interface. *Langmuir* **2002**, *18* (17), 6478−6483.
(24) Lee, K. Y.; Bae, Y.; Kim, M.; Cheong, G. W.; Kim, J.; Lee, S. S.; Han, S. W. Crown ether derivatives-mediated self-assembly of nanoparticles at the liquid/liquid interface. *Thin Solid Films* **2006**, *515* (4), 2049−2054.
(25) Lee, K. Y.; Cheong, G. W.; Han, S. W. C-60-mediated self-assembly of gold nanoparticles at the liquid/liquid interface. *Colloids Surf., A* **2006**, *275* (1−3), 79−82.
(26) Lepkova, K.; Clohessy, J.; Cunnane, V. J. The pH-controlled synthesis of a gold nanoparticle/polymer matrix via electrodeposition at a liquid-liquid interface. *J. Phys.: Condens. Matter* **2007**, *19* (37), 375106.
(27) Lepkova, K.; Clohessy, J.; Cunnane, V. J. Electrodeposition of metal-based nanocomposites at a liquid-liquid interface controlled via the interfacial Galvani potential difference. *Electrochim. Acta* **2008**, *53* (21), 6273−6277.
(28) Luo, K.; Schroeder, S. L. M.; Dryfe, R. A. W. Formation of Gold Nanocrystalline Films at the Liquid/Liquid Interface: Comparison of Direct Interfacial Reaction and Interfacial Assembly. *Chem. Mater.* **2009**, *21* (18), 4172−4183.
(29) Sanyal, M. K. The use of grazing incidence X-ray scattering techniques to probe chemical reactions at the liquid-liquid interface: the formation and ordering of gold nanoparticles. *J. Mater. Chem.* **2009**, *19* (25), 4300−4306.
(30) Selvakannan, P. R.; Mandal, S.; Pasricha, R.; Adyanthaya, S. D.; Sastry, M. One-step synthesis of hydrophobized gold nanoparticles of controllable size by the reduction of aqueous chloroaurate ions by hexadecylaniline at the liquid-liquid interface. *Chem. Commun.* **2002**, *13*, 1334−1335.
(31) Su, B.; Abid, J. P.; Fermin, D. J.; Girault, H. H.; Hoffmannova, H.; Krtil, P.; Samec, Z. Reversible voltage-induced assembly of Au nanoparticles at liquid vertical bar liquid interfaces. *J. Am. Chem. Soc.* **2004**, *126* (3), 915−919.
(32) Swami, A.; Kumar, A.; D'Costa, M.; Pasricha, R.; Sastry, M. Variation in morphology of gold nanoparticles synthesized by the spontaneous reduction of aqueous chloroaurate ions by alkylated tyrosine at a liquid-liquid and air-water interface. *J. Mater. Chem.* **2004**, *14* (17), 2696−2702.
(33) Mirceski, V.; Gulaboski, R. Simple electrochemical method for deposition and voltammetric inspection of silver particles at the liquid-liquid interface of a thin-film electrode. *J. Phys. Chem. B* **2006**, *110* (6), 2812−2820.
(34) Platt, M.; Dryfe, R. A. W. Structural and electrochemical characterisation of Pt and Pd nanoparticles electrodeposited at the liquid/liquid interface: Part 2. *Phys. Chem. Chem. Phys.* **2005**, *7* (8), 1807−1814.
(35) Platt, M.; Dryfe, R. A. W. Electrodeposition at the liquid/liquid interface: The chronoamperometric response as a function of applied potential difference. *J. Electroanal. Chem.* **2007**, *599* (2), 323−332.
(36) Platt, M.; Dryfe, R. A. W.; Roberts, E. P. L. Controlled deposition of nanoparticles at the liquid-liquid interface. *Chem. Commun.* **2002**, *20*, 2324−2325.
(37) Johans, C.; Clohessy, J.; Fantini, S.; Kontturi, K.; Cunnane, V. J. Electrosynthesis of polyphenylpyrrole coated silver particles at a liquid-liquid interface. *Electrochem. Commun.* **2002**, *4* (3), 227−230.
(38) Komsiyska, L.; Staikov, G. Electrocrystallization of Au nanoparticles on glassy carbon from HClO4 solution containing [AuCl4](-). *Electrochim. Acta* **2008**, *54* (2), 168−172.
(39) Sandmann, G.; Dietz, H.; Plieth, W. Preparation of silver nanoparticles on ITO surfaces by a double-pulse method. *J. Electroanal. Chem.* **2000**, *491* (1−2), 78−86.
(40) Ueda, M.; Dietz, H.; Anders, A.; Kneppe, H.; Meixner, A.; Plieth, W. Double-pulse technique as an electrochemical tool for controlling the preparation of metallic nanoparticles. *Electrochim. Acta* **2002**, *48* (4), 377−386.
(41) Brülle, T.; Ju, W.; Niedermayr, P.; Denisenko, A.; Paschos, O.; Schneider, O.; Stimming, U. Size-Dependent Electrocatalytic Activity of Gold Nanoparticles on HOPG and Highly Boron-Doped Diamond Surfaces. *Molecules* **2011**, *16* (12), 10059−10077.
(42) Ye, F.; Li, J.; Wang, T.; Liu, Y.; Wei, H.; Li, J.; Wang, X. Electrocatalytic Properties of Platinum Catalysts Prepared by Pulse

Electrodeposition Method Using SnO2 as an Assisting Reagent. *J. Phys. Chem. C* **2008**, *112* (33), 12894−12898.
(43) Chen, J.; Sato, M. Steady-state current at oil|water|electrode interfaces using ion-insoluble polydimethylsiloxane droplets. *J. Electroanal. Chem.* **2004**, *572* (1), 153−159.
(44) Aoki, K.; Li, M. J.; Chen, J. Y.; Nishiumi, T. Spontaneous emulsification at oil-water interface by tetraalkylammonium chloride. *Electrochem. Commun.* **2009**, *11* (2), 239−241.
(45) Takhistov, P.; Paul, S. Formation of oil/water emulsions due to electrochemical instability at the liquid/liquid interface. *Food Biophys.* **2006**, *1* (2), 57−73.
(46) De Levie, R. Capillary response at a dropping mercury electrode. *J. Electroanal. Chem.* **1965**, *9* (2), 117−127.
(47) Alexeyeva, N.; Laaksonen, T.; Kontturi, K.; Mirkhalaf, F.; Schiffrin, D. J.; Tammeveski, K. Oxygen reduction on gold nanoparticle/multi-walled carbon nanotubes modified glassy carbon electrodes in acid solution. *Electrochem. Commun.* **2006**, *8* (9), 1475−1480.
(48) Huang, M. H.; Shen, Y.; Cheng, W. L.; Shao, Y.; Sun, X. P.; Liu, B. F.; Dong, S. J. Nanocomposite films containing Au nanoparticles formed by electrochemical reduction of metal ions in the multilayer films as electrocatalyst for dioxygen reduction. *Anal. Chim. Acta* **2005**, *535* (1−2), 15−22.
(49) Lueck, H. B.; Daniel, D. C.; McHale, J. L. Resonance Raman study of solvent effects on a series of triarylmethane dyes. *J. Raman Spectrosc.* **1993**, *24*, 363.